Configurational entropy measurements in extremely supercooled liquids that break the glass ceiling

Ludovic Berthier[a,1], Patrick Charbonneau[b,c,1,2], Daniele Coslovich[a,1], Andrea Ninarello[a,1], Misaki Ozawa[a,1], and Sho Yaida[b,1]

[a]Laboratoire Charles Coulomb, UMR 5221 CNRS, Université de Montpellier, 34095 Montpellier, France; [b]Department of Chemistry, Duke University, Durham, NC 27708; and [c]Department of Physics, Duke University, Durham, NC 27708

Edited by Pablo G. Debenedetti, Princeton University, Princeton, NJ, and approved September 11, 2017 (received for review April 25, 2017)

Liquids relax extremely slowly on approaching the glass state. One explanation is that an entropy crisis, because of the rarefaction of available states, makes it increasingly arduous to reach equilibrium in that regime. Validating this scenario is challenging, because experiments offer limited resolution, while numerical studies lag more than eight orders of magnitude behind experimentally relevant timescales. In this work, we not only close the colossal gap between experiments and simulations but manage to create in silico configurations that have no experimental analog yet. Deploying a range of computational tools, we obtain four estimates of their configurational entropy. These measurements consistently confirm that the steep entropy decrease observed in experiments is also found in simulations, even beyond the experimental glass transition. Our numerical results thus extend the observational window into the physics of glasses and reinforce the relevance of an entropy crisis for understanding their formation.

glass | relaxation | entropy | simulation

In his landmark 1948 paper, Kauzmann (1) gathered experimental data for several glass-forming liquids and found that they all showed a steep decrease of their equilibrium configurational entropy on lowering temperature toward their glass transition. Theoretically, the nature of a thermodynamic glass transition associated with a vanishing configurational entropy is well-understood at the mean-field level (2–4), suggesting that glass formation is accompanied by a rarefaction of available disordered states (5). Its pertinence beyond the mean-field framework, however, remains controversial (5–8). In particular, it is still not known whether such entropy reduction is the core explanation for glass formation. Experimental measurements are carried out over too limited a temperature range within boundaries that have remained essentially unchanged since Kauzmann's work and, thus, form a solid glass ceiling. In addition, experimental determinations of the configurational entropy are marred by approximations that influence their physical interpretation (9–11). Computer simulations can potentially provide more precise estimates (12, 13) but have so far been restricted to a temperature range that is not experimentally relevant.

Can the debate over the role of configurational entropy ever be settled? At first sight, closure seems unlikely for two main reasons. (*i*) Measuring the configurational entropy below the experimental glass transition seems logically impossible, because experiments are constrained by their own duration, which fixes an upper limit to the accessible thermalization timescale, τ. Specifically, $\tau/\tau_0 \sim 10^{13}$ for molecules (14) (where the relaxation time at the onset temperature is $\tau_0 \approx 10^{-10}$s), and $\tau/\tau_0 \sim 10^5$ for colloids (15) (where $\tau_0 \approx 10^{-1}$s). The situation for computer simulations is even worse. Current approaches access at most $\tau/\tau_0 \sim 10^5$, which is eight orders of magnitude behind molecular liquid experiments, and numerical progress has been slow. The two to three decades gained over the past 35 years (15–17) are mostly thanks to hardware improvements. At this pace, another century would be needed before simulations attain experimentally relevant conditions. The glass ceiling, therefore, seems unbreakable. (*ii*) There is a fundamental methodological ambiguity as to which configurational entropy should be measured to match theoretical calculations. Qualitatively, the configurational entropy is defined by subtracting vibrational contributions from the total entropy (1, 12, 18). What is specifically meant by "vibrations" in amorphous solids, however, is ill-defined in general (5) and difficult to measure in practice (1, 13). Hence, consistently determining the configurational entropy is in itself a difficult challenge that may be underestimated in the literature.

Here, we solve both of these major problems at once. First, we take advantage of the flexibility offered by computer simulations to dramatically accelerate the equilibrium sampling of configuration space (19–21). Namely, we use a system optimized for the nonlocal swap Monte Carlo (MC) algorithm, which enables its extremely fast thermalization. We establish that this approach surpasses any current alternative and even experimental protocols. Second, we measure four proxies for the configurational entropy by deploying state of the art computational tools to characterize in silico configurations that are more deeply equilibrated than their experimental analogs (13, 20, 22, 23) and obtain consistent results that have a clear physical interpretation. By combining these developments for a realistic model glass former, we shift computer simulations from lagging eight decades behind

Significance

Computer simulations give precious insight into the microscopic behavior of disordered and amorphous materials, but the timescales they cover are orders of magnitude shorter than in experiments. For instance, simulations of glass-forming liquids cover at most 4–5 decades of viscous slowing down, which fall far short of the 12–13 decades commonly accessible in experimental studies. We here close this enormous gap for some realistic liquid models, and even equilibrate beyond experimental timescales by means of the swap Monte Carlo algorithm. We show that the approach to the glass phase is accompanied by a precipitous decrease of the configurational entropy as well as by growing spatial correlations, which we visualize in real space under experimentally relevant conditions.

Author contributions: L.B., P.C., D.C., A.N., M.O., and S.Y. designed research, performed research, analyzed data, and wrote the paper.

The authors declare no conflict of interest.

This article is a PNAS Direct Submission.

Data deposition: The data necessary to reproduce the figures in this paper are publicly available through the Duke University Libraries Digital Repository (https://doi.org/10.7924/G8ZG6Q9T).

[1]L.B., P.C., D.C., A.N., M.O., and S.Y. contributed equally to this work.

[2]To whom correspondence should be addressed. Email: patrick.charbonneau@duke.edu.

This article contains supporting information online at www.pnas.org/lookup/suppl/doi:10.1073/pnas.1706860114/-/DCSupplemental.

experiments to exploring unexpected territory in glass physics. In particular, our measurements validate Kauzmann's observations that the configurational entropy decreases steeply toward the glass temperature and extend these observations to a regime previously inaccessible.

Results

We simulate a 3D polydisperse mixture of hard spheres, as in ref. 20, which is a good model for colloids used in experiments (15, 24). We show in *SI Appendix* that our methods and conclusions also apply to particles with soft and more complex interactions. We control the volume fraction ϕ and measure pressure P to report the (unitless) reduced pressure, $Z = P/(\rho k_B T)$, where ρ is the number density and $k_B T$ is the thermal energy. This natural control variable for hard spheres plays a role akin to the inverse temperature in thermal liquids (25). Detailed information about the simulations is provided in *Model* and *Methods*. Swap MC complements standard translational MC moves with nonlocal moves that exchange randomly chosen pairs of particles, ensuring equilibrium sampling. Detailed tests of thermalization of all glassy degrees of freedom are reported in *SI Appendix* (21). We show the extreme speedup actually achieved by swap MC for this model in Fig. 1, in which the structural relaxation time τ for both MC sampling methods is reported as the system approaches its glass transition. Note that the rapid increase of τ in standard MC simulations resembles the fragile super-Arrhenius behavior of standard glass formers (5). We can only indirectly assess fragility beyond the reported numerical regime, which we estimated to be $m \approx 50$. We have fitted several empirical forms to our measurements, which thermalize up to $Z \approx 27$, to estimate the experimental glass transition at $\tau/\tau_0 = 10^{13}$. Use of various fits reflects the well-known uncertainties associated with the empirical description of data measured over a large dynamical range (26). The fits nonetheless give consistent locations for the glass ceiling, $Z_g \approx 32$–34, as highlighted in Fig. 1. Remarkably, this dramatic slowdown is completely bypassed by swap MC sampling, which thermalizes the system up to $Z \approx 38 > Z_g$. Even the most conservative extrapolation indicates that we access a dynamical range that is broader than in experiments. Meanwhile, the two-point structure barely budges (Fig. 1 *B* and *C*), which is a telltale sign of glassiness (5) and a confirmation that both crystallization and more subtle fractionation effects are absent. Visual inspection of particle configurations further confirms these conclusions (Fig. 1 *D* and *E*). We are, therefore, in the unique position of studying at equilibrium a homogeneous supercooled liquid beyond the experimental glass ceiling.

We then turn to measuring the configurational entropy, $s_{\rm conf}$, in these extremely supercooled configurations. The numerical procedures leading to the four estimates of $s_{\rm conf}$ are shown in Fig. 2. Additional details are provided in *SI Appendix*. In method 1, we determine the configurational entropy from its most conventional definition, $s_{\rm conf} = s_{\rm tot} - s_{\rm vib}$, as used in many experimental and simulation studies (1, 12, 18, 22). The total entropy of the equilibrium fluid, $s_{\rm tot}$, is measured by thermodynamic integration from the dilute ideal gas limit to the target volume fraction, while the vibrational contribution, $s_{\rm vib}$, is measured by Frenkel–Ladd thermodynamic integration (22, 27). The latter integration is over the amplitude of the Hookean constant, α, of a spring that constrains each particle to reside close to the position of a quenched reference equilibrium configuration. This requires estimating the mean-squared distance δr^2 between the reference and constrained systems over a broad range of α values, as illustrated in Fig. 2*A*. In continuously polydisperse systems, special care is also needed to account for the mixing contribution to the total entropy, because this contribution formally diverges (28, 29). The mixing entropy is thus determined from an independent, additional set of simulations (29) (*SI Appendix*). Note that method 1 is equivalent to partitioning configuration space into basins of attraction of inherent structures (7). The resulting estimate of the configurational entropy thus counts the number of energy minima (12, 30), which presumably overestimates the number of relevant basins in the free energy landscape (31).

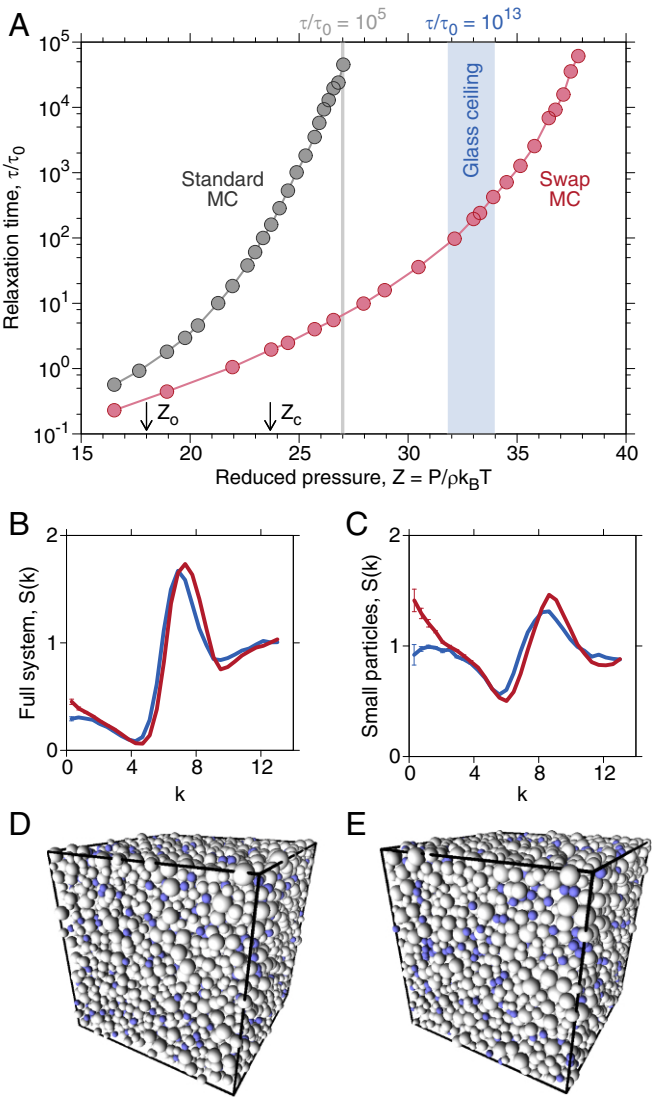

Fig. 1. Breaking the glass ceiling: thermalization beyond the experimental glass transition. (*A*) Structural relaxation time, τ, for both standard and accelerated swap MC dynamics as a function of the reduced pressure of a polydisperse hard sphere model, where τ is obtained from the decay of the self-intermediate scattering function at a wavenumber $k = 5.25$. The onset of slow dynamics occurs at $Z_0 \approx 18$, and the mode-coupling cross-over is at $Z_c \approx 23.5$. Times are rescaled by $\tau_0 = \tau(Z_0)$ for standard MC. The current limits of colloidal ($\tau/\tau_0 = 10^5$) and molecular ($\tau/\tau_0 = 10^{13}$) experiments are indicated by vertical bands (the uncertainty stems from the extrapolation scheme), showing that swap MC breaks the glass ceiling. Static structure factor for $Z = 18.8 \approx Z_0$ ($\phi = 0.568$) and $Z = 33.2$ ($\phi = 0.640$) for (*B*) all particles and (*C*) the 40% of particles with the smallest diameters. *D* and *E* show typical snapshots for these two state points, where the smallest particles are highlighted in blue.

Methods 2 and 3 are both based on the Franz–Parisi theoretical construction (32), which expresses the equilibrium free energy of the liquid, $V(Q)$, in terms of a global order parameter, the overlap Q. The overlap between two configurations is defined as $Q = N^{-1} \sum_{i,j} \theta(a - |\mathbf{r}_{1,i} - \mathbf{r}_{2,j}|)$, where $\theta(x)$ is

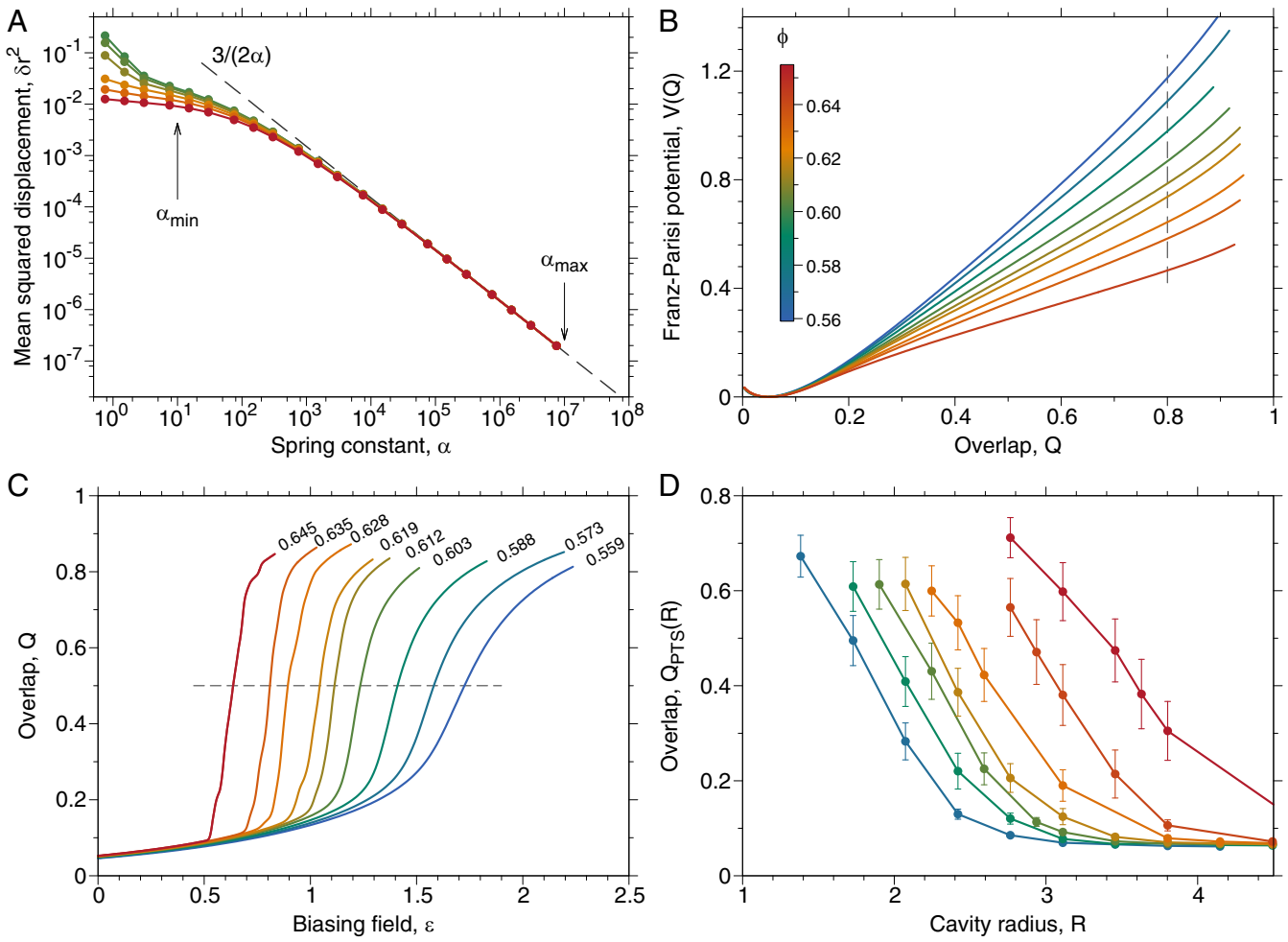

Fig. 2. Numerical procedures leading to the four estimates of the configurational entropy. (*A*) Method 1. The Frenkel–Ladd method to obtain the vibrational entropy s_{vib} performs a thermodynamic integration of the mean-squared distance δr^2 between a reference equilibrium configuration and a copy of the system constrained by a harmonic potential of strength α. The integration is carried out from α_{max}, for which the system behaves as an Einstein solid (indicated by the dashed line $\delta r^2 = 3/(2\alpha)$), to α_{min}, for which particles are trapped by their own cages on the vibrational timescale. (*B*) Method 2. The numerically determined Franz–Parisi potential $V(Q)$ is used to measure the configurational entropy as $s_{conf} = V(Q_{high} = 0.8) - V(Q_{low} \approx 0.05)$. (*C*) Method 3. The evolution of the overlap Q with the biasing field ε reveals a first-order jump at a value $\varepsilon^\star$, for which $Q = 1/2$ (dashed line). Then, $s_{conf} = \varepsilon^\star(Q_{high} - Q_{low})$. (*D*) Method 4. The decay of the cavity overlap correlation function $Q_{PTS}(R)$ with cavity radius, R, defines the point-to-set correlation length $\xi_{PTS} \propto s_{conf}^{-1/(d-\theta)}$.

the Heaviside function, $\mathbf{r}_{1,i}$ and $\mathbf{r}_{2,j}$ are the positions of particles i and j within configurations 1 and 2, respectively, and a is a fraction of the average particle diameter. By definition, Q quantifies the similarity between the coarse-grained density profiles of two configurations. To compute $V(Q)$, we introduce a coupling between a quenched reference equilibrium configuration and a copy of the system through a field ε conjugate to Q (13, 32); ε constrains the collective density profile, whereas α in method 1 constrains single-particle displacements. We define $V(Q) = -\lim_{\varepsilon\to 0}[T/N \ln P(Q)]$, where $P(Q)$ is the equilibrium probability distribution of the overlap for a given reference configuration, and brackets denote averaging over these configurations. In method 2, we follow ref. 13 and use the free energy difference $s_{conf} = V(Q_{high}) - V(Q_{low})$ between the global minimum at $Q_{low} \approx 0.05$ and its value at $Q_{high} = 0.8$ to obtain an estimate of s_{conf} that is closest to its theoretical definition (Fig. 2*B*). Importantly, this estimate only exists for sufficiently supercooled states, for which Q_{high} can be defined (13). For our system, this happens close to the mode-coupling cross-over, Z_c. In method 3, we determine the value of the biasing ε needed to "tilt" the potential $V(Q)$, so that a first-order phase transition, at which Q jumps from Q_{low} to Q_{high}, takes place as illustrated in Fig. 2*C*. We use the maximum variance of the overlap fluctuations to measure $\varepsilon^\star$ for each volume fraction studied. In practice, this is equivalent to determining the biasing field at which the overlap reaches $Q = 1/2$ (Fig. 2*C*).

Method 4 builds on the physical idea that the decrease of the configurational entropy is directly responsible for the growth of spatial correlations quantified by the point-to-set correlation length, ξ_{PTS} (33–35). Following what is becoming common practice (23, 35), we measure ξ_{PTS} by pinning the position of particles outside a spherical cavity of radius R, equilibrating the liquid within it, and measuring the evolution of the overlap between interior configurations, $Q_{PTS}(R)$, with the cavity radius R, as shown in Fig. 2*D*. The decay of $Q_{PTS}(R)$ is controlled by ξ_{PTS}, and the variance of the overlap fluctuations also presents a maximum (23) very close to ξ_{PTS}. Physically, ξ_{PTS} thus represents the cavity size above which the system starts to explore a significant number of distinct states. With minimal hypothesis (34), it can be connected to the configurational entropy through $s_{conf} \propto \xi_{PTS}^{-(d-\theta)}$, with an unknown exponent $\theta \leq (d-1)$. Various values of θ have been proposed, including $\theta = 2$ from saturating

the inequality (37) and $\theta = 3/2$ from a wetting argument (6, 36). Because our measurements are consistent with both of these values, we cannot unambiguously distinguish one proposal from the other.

We gather the four estimates of the configurational entropy in Fig. 3 to produce a plot akin to the original 1948 Kauzmann representation of $s_{\rm conf}(T)$ (1). Although in the high-temperature liquid, the configurational entropy is not sensibly defined (13), three of the four measures can still be estimated. Note that only this regime was accessible in earlier simulations (12, 13, 22). In the more relevant low-temperature regime, our main finding is that the important conceptual and technical differences between the four methods nevertheless result in qualitatively consistent results. In particular, the three estimates (methods 2–4) that closely follow the theoretical definition of the configurational entropy provide numerically indistinguishable results at low temperatures. The conventional estimate of the entropy (method 1) is larger, as expected (31), but its temperature evolution remains qualitatively consistent with the other methods. All of our estimates of $s_{\rm conf}$ thus exhibit a steep decrease as Z increases toward the glass phase, which is consistent with the seemingly fragile behavior of the model in Fig. 1. Although a quantitative extrapolation is hard to control, our measurements robustly suggest that $s_{\rm conf}$ may vanish near $Z \approx 1/0.022 \approx 45$. We thus conclude that, even for a simple glass-forming system equilibrated deeper in the landscape than any previously studied material, the trend discovered 70 years ago by Kauzmann is confirmed when more precise estimates of $s_{\rm conf}$ are adopted and persists below the experimental glass temperature.

We further show in *SI Appendix* that similar observations can be made for a model with a continuous pair potential, suggesting that our methodological progress and physical conclusions are not restricted to hard spheres and likely apply more generally. Note that, while continuous polydisperse distributions are commonplace in colloidal suspensions, a molecular liquid with a sufficiently large number of components to approximate a continuous size distribution has yet to be considered.

Discussion

Our point-to-set measurements go beyond Kauzmann's observation by establishing that the decrease in $s_{\rm conf}$ is accompanied by an increase of static spatial correlations as the glass ceiling is crossed. This result reinforces a recent experimental report based on nonlinear dielectric measurements (38). In absolute value, the measured static length scale at the experimental glass transition appears somewhat smaller than previous estimates based on dynamical correlations (39, 40) but remains compatible with the modest growth expected from general arguments based on thermally activated scaling (6, 34, 36) and decorrelation between static and dynamical length scales (41). Our particle-based resolution of such correlations further provides a direct visualization of the spatial profile of the overlap within a spherical cavity (Fig. 3, *Inset*). In particular, within a cavity comprising about 200 particles, the positions of particles freely fluctuate near the onset pressure but become strongly correlated over the entire cavity for the largest pressure shown. The spatial extent of static correlations is thus directly revealed.

The important methodological advances achieved here regarding the thermalization of supercooled liquids and the measurement of configurational entropy, therefore, support a thermodynamic view of the glass formation based on the rarefaction of metastable state accompanied by growing static correlations that is devoid of the experimental ambiguities and that extends to a temperature regime which has never been explored before.

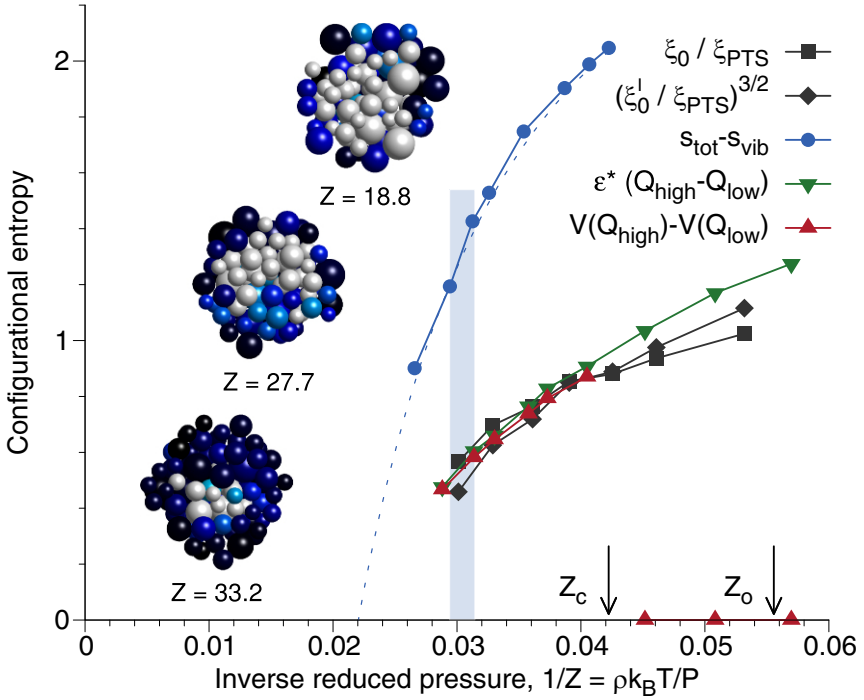

Fig. 3. Convergent measurements of the four estimates of the configurational entropy beyond the glass ceiling; $s_{\rm conf}$ is plotted as a function of $1/Z \propto T/P$, which is equivalent to the classic Kauzmann plot. All measurements indicate a steep decrease of $s_{\rm conf}$ that continues as the experimental glass ceiling is crossed. The point-to-set estimates are normalized with $\xi_0 = 2.0$ for $\theta = 2$ and $\xi_0' = 2.1$ for $\theta = 3/2$ to match the Franz–Parisi estimates at the start of the low-temperature regime, $1/Z = 0.04 \approx 1/Z_c$. The dashed line is an extrapolation based on $s_{\rm tot} - s_{\rm vib}$ (*SI Appendix*). (*Inset*) Typical overlap profiles measured in a finite cavity of radius $R = 3.46$, with colors coding for the overlap value from low (white) to large (black). Overlap fluctuations are uncorrelated around the onset but become strongly correlated over the entire cavity at the largest pressure shown.

Materials and Methods

Model. We study a 3D hard sphere model, for which the pair interaction is zero for nonoverlapping particles and infinite otherwise. Systems have a continuous size polydispersity, with particle diameters σ randomly drawn from the distribution $f(\sigma) = A\sigma^{-3}$ with $\sigma \in [\sigma_{\min}, \sigma_{\max}]$ with normalization constant A. Our model is the same as that studied in ref. 20, with a measure of size polydispersity $\Delta = \sqrt{\overline{\sigma^2} - \overline{\sigma}^2}/\overline{\sigma}$, where $\overline{\cdots} = \int d\sigma f(\sigma)(\cdots)$, $\Delta = 23\%$, and $\sigma_{\min}/\sigma_{\max} = 0.4492$. The average diameter, $\overline{\sigma}$, defines the unit of length. We simulate systems composed of N particles in a cubic cell of volume V under periodic boundary conditions (42). Depending on the method chosen to estimate the configurational entropy (*SI Appendix*), we simulate systems with $N = 1{,}000$, $N = 8{,}000$ (method 1), or $N = 300$ (methods 2 and 3). Cavities for method 4 are carved from bulk configurations with $N = 8{,}000$. The relaxation times shown in Fig. 1*A* are obtained from samples with $N = 1{,}000$. Given these parameters, the system is then uniquely characterized by its volume fraction $\phi = \pi N\overline{\sigma^3}/(6V)$, and we frequently report the data using the reduced pressure $Z = P/(\rho k_B T)$, where ρ, k_B, and T are the number density, Boltzmann constant, and temperature, respectively. Without loss of generality, we set k_B and $T = 1/\beta$ to unity. The pressure P is calculated from the contact value of the pair correlation function properly scaled for a polydisperse system (43).

Methods. To obtain equilibrium fluid configurations deep in the glassy regime, we perform MC simulations with both translational displacements and nonlocal particle swaps (19, 20, 44–50). The two types of moves are selected randomly: with probability 0.8 we attempt a translational displacement, and with probability 0.2 we attempt a swap. Translational displacements are uniformly drawn over a cube of side 0.115. For swaps, two randomly selected particles exchange diameter. In both cases, proposed moves are accepted if no overlap is created. Following ref. 21, we also immediately reject swaps between particles with diameters that differ by more than 0.2.

We measure the equilibrium relaxation time τ both with and without the swap moves from the time decay of the self-intermediate scattering function, $F_s(k, \tau) = 1/e$, where $k = 5.25$ is the wavenumber chosen slightly below the first maximum of the static structure factor. Note that the particles' diameters can change during a swap MC simulation, but their trajectories are continuous. Relaxation times are measured in units of MC sweeps, comprising N MC moves, irrespective of their type.

Thermalized systems at each state point are obtained in the same way for both standard and swap MC dynamics. We measure the relaxation time τ and ensure that, for each state point, simulations of a total duration of at least 100τ can be performed. We also check for the presence of aging effects in time correlation functions, and we measure the static structure factor, the pair correlation function, and the equation of state over long simulations, paying attention to any temporal drift that could signal improper thermalization, incipient crystallization, or demixing of particles with distinct sizes. Selected results for the evolution of the structure factor with volume fraction are presented in Fig. 1 *B* and *C*. Over the extreme range of densities shown here, the static structure evolves very little. Similarly, a very modest evolution is seen when the partial structure factor of the smallest particles is measured. A large increase of the low-k value of these quantities or the emergence of discrete peaks would signal that demixing or crystallization is taking place. In fact, we have found that measuring the relaxation time for the swap simulation is the most sensitive test of thermalization, because purely static observables may appear thermalized over long simulation times, whereas the system is, in fact, nearly arrested in a glass state, within which sampling is inefficient.

We introduce two dynamical reference states: (*i*) the onset of slow dynamics at $\phi_0 \approx 0.56$ ($Z_0 \approx 18$), above which the time decay of correlation functions is nonexponential (51), and (*ii*) the mode-coupling cross-over $\phi_c \approx 0.598$ ($Z_c \approx 23.5$), at which a power law fit extrapolates a divergence of the relaxation times (20). Note that these particular definitions are not unique (52) but are sufficiently accurate for their purpose as qualitative references.

Localization of the Glass Ceiling. In the context of this work, the glass ceiling, Z_g, is defined through the relaxation time measured at the laboratory glass transition, at which conventionally, $\tau(Z_g)/\tau_0 = 10^{13}$ (14). Because standard MC dynamics can only access relaxation times at most of order $\tau/\tau_0 = 10^5$, where $\tau_0 = 10^4$ MC sweeps is the value of τ at the onset of slow dynamics, our dynamical data must be extrapolated to locate this ceiling. We here fit measured relaxation times to various functional forms up to $\tau/\tau_0 \leq 10^5$ and then extrapolate to the vicinity of the glass ceiling. In an effort to obtain an estimate as unbiased as possible, various functional forms (5, 25) are considered. The general strategy is described here, and the details are provided as *SI Appendix*.

The first functional form is the Vogel–Fulcher–Tammann (VFT) expression:

$$\tau = \tau_\infty \exp\left[\frac{A}{(Z_{\rm vft} - Z)^\delta}\right], \qquad [1]$$

where τ_∞, A, the exponent δ, and the critical pressure $Z_{\rm vft}$ are free parameters. Whereas $\delta = 1$ is traditionally used, more recent experimental and numerical studies favor $\delta = 2$ (15, 25). Although the location of a putative divergence of τ is sensitive to the extrapolation methods (with $Z_{\rm vft} \approx 38$ for $\delta = 1$ and $Z_{\rm vft} \approx 45$ for $\delta = 2$), the location of the glass ceiling is rather robust, with both $\delta = 1$ and $\delta = 2$ yielding $Z_g \approx 32$.

The second functional form is the parabolic law proposed by Elmatad et al. (53) in the context of facilitated models (54):

$$\tau = \tau_\infty \exp\left[A(Z - Z_0)^2\right], \qquad [2]$$

where $Z_0 = 17$ is around the onset of slow dynamics. The fit is made over the range $Z > Z_0$, with the glass ceiling located at $Z_g = 34$.

The two functional forms account well for the non-Arrhenius dependence of the relaxation time data for the range $\tau/\tau_0 \leq 10^5$ (while a simple Arrhenius expression does not). The resulting values, $Z_g \approx 32$ for VFT and $Z_g = 34$ for parabolic, are thus used to delineate the location of the glass ceiling in Fig. 1.

ACKNOWLEDGMENTS. The research at Université de Montpellier was supported by funding from the European Research Council (ERC) under European Union's Seventh Framework Program FP7/2007-2013/ERC Grant 306845 and by Simons Foundation Grant 454933 (to L.B.). The research at Duke was supported by Simons Foundation Grant 454937 (to P.C.), and associated computations were carried out through the Duke Compute Cluster.

1. Kauzmann W (1948) The nature of the glassy state and the behavior of liquids at low temperatures. *Chem Rev* 43:219–256.
2. Kirkpatrick TR, Thirumalai D (1987) *p*-spin-interaction spin-glass models: Connections with the structural glass problem. *Phys Rev B* 36:5388–5397.
3. Kirkpatrick TR, Wolynes PG (1987) Stable and metastable states in mean-field potts and structural glasses. *Phys Rev B* 36:8552–8564.
4. Charbonneau P, Kurchan J, Parisi G, Urbani P, Zamponi F (2014) Fractal free energy landscapes in structural glasses. *Nat Commun* 5:3725.
5. Berthier L, Biroli G (2011) Theoretical perspective on the glass transition and amorphous materials. *Rev Mod Phys* 83:587–645.
6. Kirkpatrick TR, Thirumalai D, Wolynes PG (1989) Scaling concepts for the dynamics of viscous liquids near an ideal glassy state. *Phys Rev A* 40:1045–1054.
7. Stillinger FH (1988) Supercooled liquids, glass transitions, and the Kauzmann paradox. *J Chem Phys* 88:7818–7825.
8. Garrahan JP, Chandler D (2003) Coarse-grained microscopic model of glass formers. *Proc Natl Acad Sci USA* 100:9710–9714.
9. Dyre J (2006) Colloquium: The glass transition and elastic models of glass-forming liquids. *Rev Mod Phys* 78:953–972.
10. Wyart M (2010) Correlations between vibrational entropy and dynamics in liquids. *Phys Rev Lett* 104:095901.
11. Rabochiy P, Wolynes PG, Lubchenko V (2013) Microscopically based calculations of the free energy barrier and dynamic length scale in supercooled liquids: The comparative role of configurational entropy and elasticity. *J Phys Chem B* 117:15204–15219.
12. Sciortino F, Kob W, Tartaglia P (1999) Inherent structure entropy of supercooled liquids. *Phys Rev Lett* 83:3214–3217.
13. Berthier L, Coslovich D (2014) Novel approach to numerical measurements of the configurational entropy in supercooled liquids. *Proc Natl Acad Sci USA* 111:11668–11672.
14. Petzold N, et al. (2013) Evolution of the dynamic susceptibility in molecular glass formers: Results from light scattering, dielectric spectroscopy, and NMR. *J Chem Phys* 138:12A510.
15. Brambilla G, et al. (2009) Probing the equilibrium dynamics of colloidal hard spheres above the mode-coupling glass transition. *Phys Rev Lett* 102:085703.
16. Barrat JL, Roux JN, Hansen JP (1990) Diffusion, viscosity and structural slowing down in soft sphere alloys near the kinetic glass transition. *Chem Phys* 149:197–208.
17. Kob W, Andersen HC (1994) Scaling behavior in the β-relaxation regime of a supercooled Lennard-Jones mixture. *Phys Rev Lett* 73:1376–1379.
18. Martinez LM, Angell C (2001) A thermodynamic connection to the fragility of glass-forming liquids. *Nature* 410:663–667.
19. Grigera TS, Parisi G (2001) Fast Monte Carlo algorithm for supercooled soft spheres. *Phys Rev E* 63:045102.
20. Berthier L, Coslovich D, Ninarello A, Ozawa M (2016) Equilibrium sampling of hard spheres up to the jamming density and beyond. *Phys Rev Lett* 116:238002.
21. Ninarello A, Berthier L, Coslovich D (2017) Models and algorithms for the next generation of glass transition studies. *Phys Rev X* 7:021039.

22. Angelani L, Foffi G (2007) Configurational entropy of hard spheres. *J Phys Cond Matter* 19:256207.
23. Berthier L, Charbonneau P, Yaida S (2016) Efficient measurement of point-to-set correlations and overlap fluctuations in glass-forming liquids. *J Chem Phys* 144:024501.
24. Pusey P, Van Megen W (1986) Phase behaviour of concentrated suspensions of nearly hard colloidal spheres. *Nature* 320:340–342.
25. Berthier L, Witten TA (2009) Glass transition of dense fluids of hard and compressible spheres. *Phys Rev E* 80:021502.
26. Stickel F, Fischer EW, Richert R (1995) Dynamics of glass-forming liquids. i. temperature-derivative analysis of dielectric relaxation data. *J Chem Phys* 102:6251–6257.
27. Frenkel D, Ladd AJ (1984) New Monte Carlo method to compute the free energy of arbitrary solids. Application to the fcc and hcp phases of hard spheres. *J Chem Phys* 81:3188–3193.
28. Frenkel D (2014) Why colloidal systems can be described by statistical mechanics: Some not very original comments on the Gibbs paradox. *Mol Phys* 112:2325–2329.
29. Ozawa M, Berthier L (2017) Does the configurational entropy of polydisperse particles exist? *J Chem Phys* 146:014502.
30. Stillinger FH, Weber TA (1985) Inherent structure theory of liquids in the hard-sphere limit. *J Chem Phys* 83:4767–4775.
31. Biroli G, Monasson R (2000) From inherent structures to pure states. *Europhys Lett* 50:155–161.
32. Franz S, Parisi G (1997) Phase diagram of coupled glassy systems: A mean-field study. *Phys Rev Lett* 79:2486–2489.
33. Adam G, Gibbs JH (1965) On the temperature dependence of cooperative relaxation properties in glass-forming liquids. *J Chem Phys* 43:139–146.
34. Bouchaud JP, Biroli G (2004) On the Adam-Gibbs-Kirkpatrick-Thirumalai-Wolynes scenario for the viscosity increase in glasses. *J Chem Phys* 121:7347–7354.
35. Biroli G, Bouchaud JP, Cavagna A, Grigera TS, Verrocchio P (2008) Thermodynamic signature of growing amorphous order in glass-forming liquids. *Nat Phys* 4:771–775.
36. Lubchenko V (2015) Theory of the structural glass transition: A pedagogical review. *Adv Phys* 64:283–443.
37. Cammarota C, Cavagna A, Gradenigo G, Grigera TS, Verrocchio P (2009) Numerical determination of the exponents controlling the relationship between time, length and temperature in glass-forming liquids. *J Chem Phys* 131:194901.
38. Albert S, et al. (2016) Fifth-order susceptibility unveils growth of thermodynamic amorphous order in glass-formers. *Science* 352:1308–1311.
39. Rabochiy P, Wolynes PG, Lubchenko V (2013) Microscopically based calculations of the free energy barrier and dynamic length scale in supercooled liquids: The comparative role of configurational entropy and elasticity. *J Phys Chem B* 117:15204–15219.
40. Berthier L, et al. (2005) Direct experimental evidence of a growing length scale accompanying the glass transition. *Science* 310:1797–1800.
41. Charbonneau P, Tarjus G (2013) Decorrelation of the static and dynamic length scales in hard-sphere glass formers. *Phys Rev E* 87:042305.
42. Allen MP, Tildesley DJ (1989) *Computer Simulation of Liquids* (Oxford Univ Press, London).
43. Santos A, Yuste SB, de Haro ML (2005) Contact values of the particle-particle and wall-particle correlation functions in a hard-sphere polydisperse fluid. *J Chem Phys* 123:234512.
44. Gazzillo D, Pastore G (1989) Equation of state for symmetric non-additive hard-sphere fluids: An approximate analytic expression and new Monte Carlo results. *Chem Phys Lett* 159:388–392.
45. Sindzingre P, Massobrio C, Ciccotti G, Frenkel D (1989) Calculation of partial enthalpies of an argon-krypton mixture by npt molecular dynamics. *Chem Phys* 129:213–224.
46. Santen L, Krauth W (2001) Liquid, glass and crystal in two-dimensional hard disks. arXiv:cond-mat/0107459.
47. Pronk S, Frenkel D (2004) Melting of polydisperse hard disks. *Phys Rev E* 69: 066123.
48. Frenkel D, Smit B (2001) *Understanding Molecular Simulation* (Academic, New York), 2nd Ed.
49. Brumer Y, Reichman DR (2004) Numerical investigation of the entropy crisis in model glass formers. *J Phys Chem B* 108:6832–6837.
50. Gutiérrez R, Karmakar S, Pollack YG, Procaccia I (2015) The static lengthscale characterizing the glass transition at lower temperatures. *Europhys Lett* 111:56009.
51. Sastry S, Debenedetti PG, Stillinger FH (1998) Signatures of distinct dynamical regimes in the energy landscape of a glass-forming liquid. *Nature* 393:554–557.
52. Charbonneau P, Jin Y, Parisi G, Zamponi F (2014) Hopping and the Stokes-Einstein relation breakdown in simple glass formers. *Proc Natl Acad Sci USA* 111:15025–15030.
53. Elmatad YS, Chandler D, Garrahan JP (2009) Corresponding states of structural glass formers. *J Phys Chem B* 113:5563–5567.
54. Isobe M, Keys AS, Chandler D, Garrahan JP (2016) Applicability of dynamic facilitation theory to binary hard disk systems. *Phys Rev Lett* 117:145701.